Quantum-chromodynamic estimates for heavy-particle production

John Babcock, Dennis Sivers, and Stephen Wolfram*
High Energy Physics Division, Argonne National Laboratory, Argonne, Illinois 60439
(Received 21 November 1977)

The associated production of hadrons containing heavy quarks is studied in the framework of a model based on quark-gluon color gauge field theory [quantum chromodynamics (QCD)]. We assume that the dominant mechanism for the production of heavy quarks in real and virtual photon beams is $\gamma(Q^2)V \to c\bar{c}$ where V denotes a vector gluon and c an arbitrary heavy quark. For π, p, and $\bar{p}$ beams we consider the mechanisms $VV \to c\bar{c}$ and $q\bar{q} \to c\bar{c}$. The cross sections for the internal subprocesses are calculated at lowest order in the perturbation expansion for QCD. We include a brief discussion of higher-order corrections to our calculation.

I. INTRODUCTION

The associated production of new, heavy, flavors of quarks in photon and hadron beams affords the opportunity to study the hadronic interactions of massive quarks. A small, but growing, body of experimental information on these processes already exists. There are indications for the production of charm by virtual photons in the observation of events of the type $\mu N \to \mu\mu X$.[1] The observation of a charmed antibaryon, $\bar{\Lambda}_c(2.26)$, has been claimed in photoproduction[2] but it has not yet been possible to deduce the corresponding cross section. Indirect evidence for charm in photoproduction can be obtained from the energy dependence of $d\sigma/dt(\gamma p \to \psi p)$ near charm threshold[3] or, perhaps, from the behavior of $\sigma_{\text{tot}}(\gamma p)$.[4] There is evidence for the production of charm in hadron-hadron collisions from cosmic-ray experiments[5] but, at this time, no accelerator experiment using hadronic beams has reported a charm signal. Perhaps the most restrictive bound on this cross section comes from an emulsion exposure[6] which gives

$$\sigma(pp \to \text{charm}, X; \sqrt{s} = 25\ \text{GeV}) \lesssim 1.5\mu\text{b} \quad (90\%\ \text{C.L.}).$$

However, the observation of ψ and ψ' production in hadron beams has become quite commonplace and there has been a recent report of an enhancement, $\Upsilon(9.5)$,[7] which presumably is the harbinger of still another flavor of quark.

There have been several model calculations of the cross sections for processes involving heavy particles but there does not appear to be a theoretical consensus on what the underlying production mechanisms should be. We shall discuss here a model for the associated production of heavy quarks which is applicable either in photon-hadron or hadron-hadron collisions. We assume that the production of heavy quarks occurs through the interaction of the fundamental fields in quantum chromodynamics (QCD)—quarks and gluons—and that the cross section is dominated by the lowest-order perturbation-theory contribution. For real or virtual photons this assumption means that the dominant internal production mechanism is $\gamma(Q^2)V \to c\bar{c}$ where V is a vector gluon and c a heavy quark. In hadron-hadron collisions we assume that the important mechanisms are $VV \to c\bar{c}$ and $q\bar{q} \to c\bar{c}$ where q denotes a light quark (u, d, s). The model is largely motivated by a similar calculation of large-p_T hadron production in QCD.[8,9] A naive justification for the approach can be found if the threshold invariant mass of the produced hadrons which carry the new flavor is large enough that the renormalization-group-improved QCD coupling constant $\alpha_s(k^2)$ is small. In practice, the requirement that $\alpha_s(m_{\text{th}}^2)$ be small may be satisfied in the production of charm or of a heavier flavor such as that associated with the $\Upsilon(9.5)$. One advantage of treating simultaneously photon-hadron and hadron-hadron collisions is that the dependence of the cross section on the main input to the calculation, the distribution $G_{V/N}(x)$ of gluons in a hadron, is different in the two cases.

The outline of the rest of this paper is as follows: In Sec. II, we discuss our calculation for photon-hadron collisions and introduce in more detail the assumptions we make. The different gluon distributions used in the calculation are presented and we make several comparisons between our calculations and those based on the generalized-vector-meson-dominance model. In Sec. III, we present our calculations for hadron-hadron collisions. The constraints on our model from the experimental bound (1.1) are discussed. Section IV gives a brief discussion of possible effects associated with higher-order corrections to our calculation. We include appendices which give the details of our perturbation-theory calculations of $\gamma(Q^2)V \to c\bar{c}$, $VV \to c\bar{c}$, and $q\bar{q} \to c\bar{c}$.

II. REAL AND VIRTUAL PHOTOPRODUCTION

In this section we will discuss the associated production of heavy hadrons carrying new flavors by real and virtual photons. Some experimental information on the photoproduction of charm already exists. The observation of a charmed antibaryon[2] provides direct evidence for the production of charm by real photons although the rate is not yet known. Indirect evidence for a charm signal comes from the observed energy dependence of $d\sigma/dt(\gamma p \to \psi p)$ near the threshold for charmed-hadron production.[3] Arguments based on generalized vector-meson dominance allow an estimate for the cross section[10] while unitarity and the Okubo-Zweig-Iizuka (OZI)[11] rule provide a lower bound on this quantity.[12]

Virtual photons should also be effective in producing charm or other heavy flavors and there exists some evidence for the production of charm in this manner from the observation of events of the type $\mu N \to \mu\mu X$.[1] A knowledge of the size and Q^2 dependence of this cross section is important in determining whether charm production is an important background at small Bjorken x to the scaling violations in $d\sigma(\mu N \to \mu X)$ expected in field theories of the strong interactions.

The basic calculation

We shall discuss our calculation of the cross section for the photoproduction of heavy particles in some detail in order to illustrate the techniques and assumptions used. Our starting point involves the diagrams of Fig. 1, where V is a vector gluon and c denotes any heavy quark. We shall tend to refer to this below as charm, but our results should also apply to the production of heavier quarks. These diagrams constitute the first-order perturbation-theory approximation in QCD to the associated production of free charmed quarks. In order to relate this to an observable cross section we assume that the outgoing charmed quarks are dressed to form charmed hadrons with unit probability, independent of their momenta. We also assume that no other flavor of quark may dress to form a charmed hadron. We further assume the mechanism by which quarks are forged into hadrons is sufficiently soft that the invariant mass of the $c\bar{c}$ pair is approximately the effective mass of the charmed hadron system containing them. The threshold invariant mass μ_{th} can then be taken to be either $2m_D$ or $(m_c - m_N + m_D)$ (corresponding roughly to the associated production process $\gamma^* N \to CD$ where C is the lightest charmed baryon) rather than being given by the effective quark masses appearing in the matrix element.

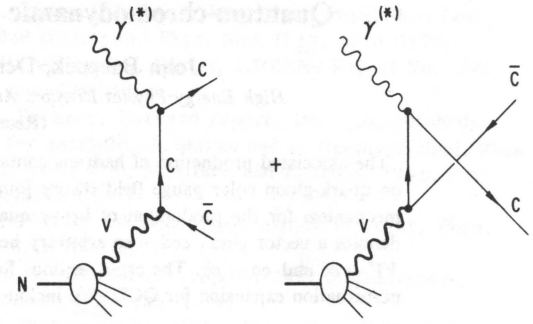

FIG. 1. Diagrams for $\gamma^* N \to c\bar{c}$ in QCD perturbation theory.

For charm production we take

$$\mu_{th}^2 \cong 13 \text{ GeV}^2 . \tag{2.1}$$

If we define the probability that a gluon carries a fraction x momentum of the nucleon which contains it to be $G_{V/N}(x)$ we can write the cross section defined by the diagrams in Fig. 1 as

$$\sigma(\gamma_T(Q^2)N \to c\bar{c}, X) \simeq \int_{x_{min}}^{1} dx\, G_{V/N}(x) \times \int_{\hat{t}_{min}}^{\hat{t}_{max}} \frac{d\hat{t}}{16\pi} \frac{1}{(\hat{s}+Q^2)^2} \times |\bar{M}(\hat{s},\hat{t},\hat{u})|^2 , \tag{2.2}$$

where

$$\hat{s} \simeq -Q^2 + 2x m_N \nu \geq \mu^2 ,$$

$$\hat{t}_{min}^{max} = -\tfrac{1}{2}(\hat{s}+Q^2-2m_c^2) \pm \frac{\hat{s}+Q^2}{2\hat{s}}[\hat{s}(\hat{s}-4m_c^2)]^{1/2} , \tag{2.3}$$

$$\hat{s}+\hat{t}+\hat{u} = 2m_c^2 - Q^2 ,$$

and

$$x_{min} = \left(\frac{\mu^2+Q^2}{2m_N\nu}\right).$$

For simplicity we consider the photoproduction of heavy quarks only from transverse photons. In the deep-inelastic region this corresponds to calculating the effect of charm production on the structure function $W_1(x,Q^2)$. In the spirit of the parton model we assume that the gluon is on its mass shell. The calculation of the spin-averaged, color-averaged $|\bar{M}(\hat{s},\hat{t},\hat{u})|^2$ for the subprocess $\gamma_T(Q^2)V \to c\bar{c}$ is given in Appendix A. The result is

$$|\bar{M}(\hat{s},\hat{t},\hat{u})|^2 = \langle\tfrac{1}{2}\rangle(\tfrac{1}{4})(\tfrac{2}{3}eg)^2(\hat{t}-m_c^2)^{-2}(\hat{u}-m_c^2)^{-2}$$
$$\times\Big(\{-(\hat{t}-\hat{u})^4-4(\hat{s}+Q^2)(\hat{t}+\hat{u})(\hat{t}-\hat{u})^2-4(\hat{s}+Q^2)^2[(\hat{t}-\hat{u})^2+2(\hat{t}+\hat{u})^2]-12(\hat{s}+Q^2)^3(\hat{t}+\hat{u})-3(\hat{s}+Q^2)^4\}$$
$$+\frac{Q^2}{\hat{s}+Q^2}[2(\hat{t}-\hat{u})^4+8(\hat{s}+Q^2)(\hat{t}+\hat{u})(\hat{t}-\hat{u})^2+8(\hat{s}+Q^2)^2(\hat{t}-\hat{u})^2-2(\hat{s}+Q^2)^4]$$
$$+\Big(\frac{Q^2}{\hat{s}+Q^2}\Big)^2[-2(\hat{t}-\hat{u})^4+2(\hat{s}+Q^2)^4]\Big). \tag{2.4}$$

For $Q^2=0$, the expression (2.4) reduces to that given by Jones and Wyld.[13] Except for the overall factors $\langle\frac{1}{2}\rangle$, (due to color averaging) and $(\frac{2}{3}g/e)^2$ the cross section is the same as that for the process $\gamma_T(Q^2)\gamma \to e\bar{e}$.

To evaluate the cross section given by (2.2) we must choose a value for g, the QCD effective coupling constant and a form for $G_{V/N}(x)$. Motivated by a study of the application of QCD to similar processes, we use a running coupling constant. By allowing the coupling to be a function of the invariant mass of the exchanged quark or gluon in a given diagram we are including some contributions from a set of higher-order diagrams in our nominally lowest-order calculation. We shall allow a range of possible values for g which reflects the uncertainties in its determination,[14]

$$\alpha_s^{\max}(k^2)=\Big(\frac{g^2}{4\pi}\Big)^{\max}=\frac{0.50}{1+0.36\ln|4k^2\ (\mathrm{GeV}^2)|}\,,$$
$$\alpha_s^{\min}(k^2)=\tfrac{1}{2}\alpha_s^{\max}\,. \tag{2.5}$$

Our results are fairly insensitive to the k^2 dependence of the coupling constant. For example, in real photoproduction with $E\gamma \leq 200$ GeV, the value for the charm cross section with a running coupling constant is less than 1% lower than that with a coupling constant fixed at its threshold value, $\alpha_s(m_{\mathrm{th}}{}^2)$. The main situation in which the k^2 dependence given by (2.5) is important is thus in comparing the production of different flavors.

Gluon distributions

The most important input to our calculation (2.2) is the gluon momentum distribution, $G_{V/N}(x)$. In fact, we need to know the probability $G_{V/N}(x,Q^2)$ for a gluon to be seen by a photon of (mass)^2 $=-Q^2$ but we will defer a discussion of the scaling violations associated with the Q^2 dependence of this function until Sec. IV. From the amount of missing momentum in deep-inelastic scattering one can conclude

$$\int_0^1 xG_{V/N}(x)dx \simeq 0.5\,, \tag{2.6}$$

but there are no other experimental constraints on the gluon distribution. Since we are forced to make theoretical models for this distribution we will present results for a variety of models representing different schools of thought. The first possible choice for $G_{V/N}(x)$ is

$$G_{V/N}^{\mathrm{naive}}(x)=\frac{3}{x}(1-x)^5\,, \tag{2.7}$$

where the behavior near $x=1$ is motivated by constituent counting rules[15] and the behavior near $x=0$ by a correspondence with Regge theory.[16]

It is also possible to calculate in the spirit of the scale-invariant parton model the gluon distributions which arise from a given valence quark distribution from processes of the form shown in Fig. 2. We then have

$$G_{V/N}(x)\simeq\int_x^1\frac{dy}{y}D_{V/q}\Big(\frac{x}{y}\Big)G_{q/N}(y)\,, \tag{2.8}$$

where $D_{V/q}(z)$ is the probability that a quark emits a gluon carrying a fraction z of its momentum. Some authors would omit the factor $1/y$ which is included here to mimic the phase-space integration. A massive particle with momentum p decaying into two massless particles, gives a particle with momentum zp $(0<z<1)$ with a probability independent of z. That is, it has $D_{v/q}(z)=\mathrm{const}$. If instead, a prescription based on constituent-counting rules which ignores the complications due to the spin of quarks and gluons is used, we have $D_{V/q}(z)\sim(1-z)$. There is some uncertainty, therefore, in the exact relation between valence quark and gluon distributions in this approach. One estimate of this relation gives[14]

$$G_{V/N}^{\mathrm{brems}}(x)=12.6(1-x)^5+1.6\frac{(1-x)^7}{x}\,. \tag{2.9}$$

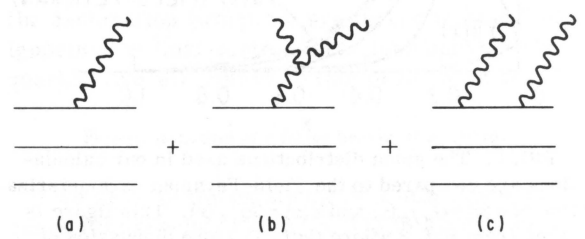

FIG. 2. Bremsstrahlung of gluons.

The overall normalization of (2.8) is determined by (2.6) while the behavior near $x = 0$ is determined by the relation between gluons and antiquarks implied by diagrams such as those in Fig. 2.

The softest gluon distribution we consider is obtained by assuming the gluons to be confined within a rigid bag of radius 0.7 fm, with normalization fixed by (2.6):

$$G^{\text{bag}}_{V/N}(x) \simeq \frac{3.8}{x} e^{-(x/0.15)^2}. \tag{2.10}$$

To obtain a significantly softer distribution would require cooperative effects among the gluons. More frequently we will use a distribution which combines the idea of nonperturbative effects with bremsstrahlung from valence quarks (which is smaller by a factor α_s/π)[14]:

$$G^{\text{bag-brems}}_{V/N}(x) = \frac{1}{x}[0.4(1-x)^4 + 3.2e^{-(x/0.15)^2}]. \tag{2.11}$$

This is only slightly different than (2.7) and represents a plausible soft distribution of gluons. The gluon distributions (2.7), (2.9), and (2.11) are shown in Fig. 3 where they are compared with a parametrization due to Field and Feynman[17] of quark and antiquark distributions.

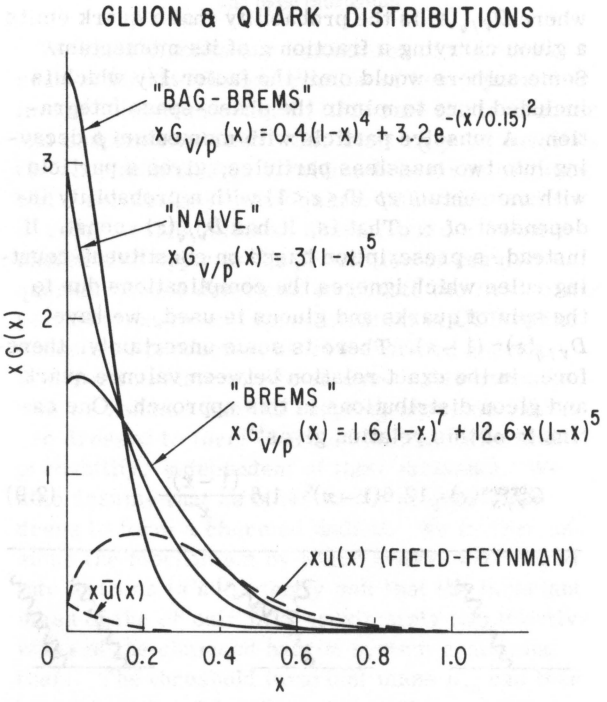

FIG. 3. The gluon distributions used in our calculations are compared to the Field-Feynman parameterization of $u(x) = G_{u/p}(x)$ and $\bar{u}(x) = G_{\bar{u}/p}(x)$. This figure is taken from Ref. 8 where there is more discussion of gluon distributions.

The results for real photoproduction

Our results for the energy dependence of the cross section for the production of charm by real photons are shown in Fig. 4. For the bag-brems gluon distribution (2.11) we show the range of predictions corresponding to our range of estimates for the strong coupling constant (2.5). For the other two gluon distributions we show only the curves corresponding to $\alpha_s = \alpha_s^{\max}$, and the range can be inferred by eye.

Also shown on the graph are some phenomenological constraints which can be used to judge the reliability of the model. Using an argument based on unitarity and the OZI rule indicated schematically in Fig. 5., one can derive the rigorous inequality[12]

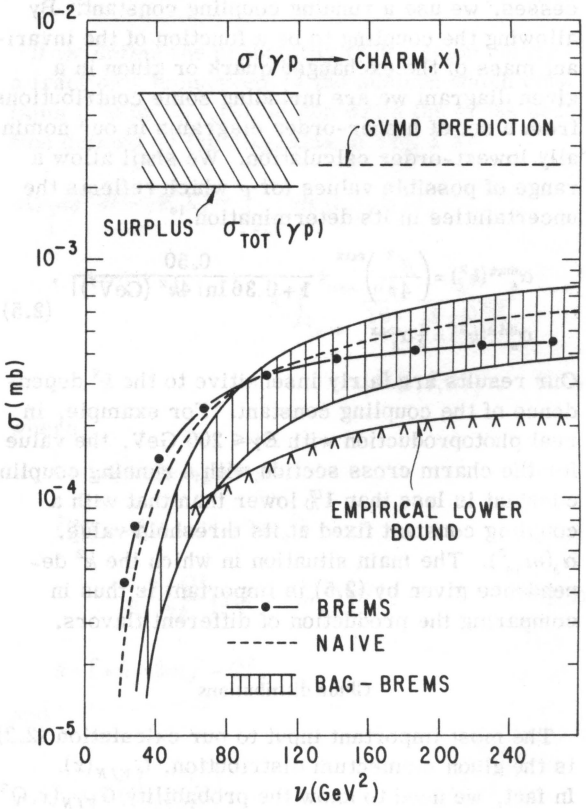

FIG. 4. Energy dependence for the cross section $\sigma(\gamma p \rightarrow \text{charm}, X)$ calculated in our model. The calculation with the bag-brems gluon distribution (2.11) is shown as a band of values corresponding to the range of α_s in (2.5). For the brems (2.9) and the naive (2.5) distributions we calculate only with $\alpha_s^{\max}$. Also shown are the range for $\sigma_{\text{tot}}(\gamma p \rightarrow \text{charm}, X)$ which might be inferred from the data on $\sigma_{\text{tot}}(\gamma p)$ of Ref. 4, a prediction of the GVMD model (Ref. 10) and a lower bound (Ref. 12) from unitarity.

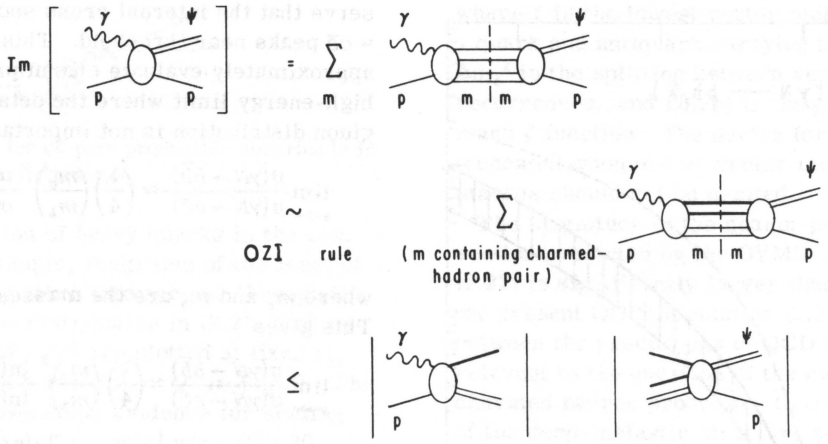

FIG. 5. Bound on charm photoproduction from unitarity and the OZI rule in ψ photoproduction.

$$16\pi\frac{d\sigma}{dt}(\gamma p\to\psi p; s, t=t_{\max})$$

$$\leq (1+\epsilon)^2(1+\rho^2)\left(\frac{q_s^{\psi p}}{q_s^{\gamma p}}\right)$$

$$\times\sigma(\gamma p\to\text{charm}, s)\sigma(\psi p\to\text{charm}, s)\,, \quad (2.12)$$

where ϵ is a parameter which measures OZI-rule violations and should be quite small, $\rho=\mathrm{Re}A/\mathrm{Im}A$ where A is the diffractive amplitude for $\gamma p\to\psi p$, and

$$\frac{q_s^{\psi p}}{q_s^{\gamma p}}=\frac{[s-(m_p+m_\psi)^2]^{1/2}[s-(m_p-m_\psi)^2]^{1/2}}{(s-m_p^2)}\,. \quad (2.13)$$

Using data[18] on $d\sigma/dt(\gamma p\to\psi p)$ and the nuclear absorption measurement[19]

$$\sigma_{\text{tot}}(\psi p)\simeq 3\text{ mb}\simeq\sigma(\psi p\to\text{charm}, X)\,, \quad (2.14)$$

Eq. (2.12) yields an empirical lower bound on the charm-photoproduction cross section. This is shown in Fig. 4.

Also shown in Fig. 4 is a band of 2–5 μb which is due to a careful experiment[4] which measures $\sigma_{\text{tot}}(\gamma p, s)$ for $E_\gamma=20$–100 GeV and compares it with an extrapolation of low-energy data. Depending slightly on the parametrization used they find a surplus in $\sigma_{\text{tot}}(\gamma p)$. One interpretation of this surplus is that it is due to charm production. Also, the generalized vector-meson-dominance (GVMD) model[10] predicts

$$\sigma_{\text{GVMD}}(\gamma p\to\text{charm})\simeq 2.5\ \mu\text{b}\,. \quad (2.15)$$

It is significant, therefore, that our QCD calculation gives results approximately a factor of 10 lower than this GVMD estimate or the surplus of the cross section observed experimentally. Our calculation is, in fact, consistent with charm production approximately saturating the lower bound derived from unitarity. The saturation of this lower bound for charm production was argued for on the basis of the photoproduction of strange particles and it is interesting that we have a calculation completely independent of $\gamma p\to\psi p$ which gives this result. Our results in Fig. 4 agree with those of Jones and Wyld[13] and we find approximate agreement with the sum rule of Shifman, Vainshtein, and Zakharov.[20]

The experimental measurement of the charm signal in γp collisions at Fermilab or the CERN SPS should therefore distinguish quite easily between the GVMD result and the range calculated here. If experiments find the lower values predicted here it would be significant support for the validity of simple QCD perturbation theory for this type of calculation. If the results of QCD are born out at high energy, we can see from Fig. 4 that a measurement of the charm signal at $E\gamma\cong 20$ GeV would be able to discriminate between the gluon distributions (2.7), (2.19), and (2.11). Since gluon distributions are not very accessible experimentally, this is a potentially valuable capability.

It is important to note that the cross section (2.6) is peaked near threshold where the outgoing charmed quarks do not have a large relative velocity. There is, therefore, little justification for the assumption (which we are forced to make) of ignoring the final-state interactions between the quarks. We will return to this problem in Sec. V.

Photoproduction of a flavor heavier than charm

If we assume the existence of a new flavor of quark (b) associated with the $\Upsilon(9.5)$ we can use our formula (2.2) to calculate the production of

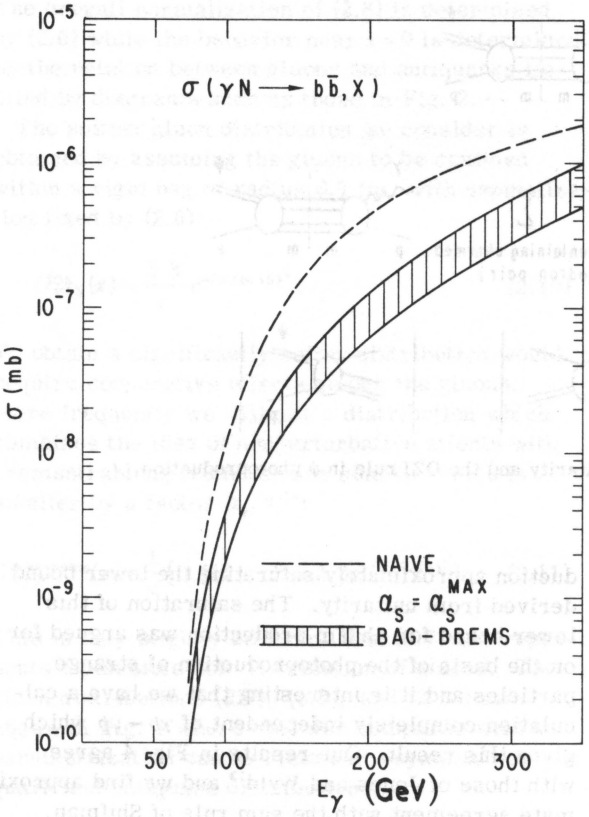

FIG. 6. The energy dependence for the cross section $\sigma(\gamma N \to b\bar{b}, X)$ calculated using (2.2)–(2.5) with $m_b = 5$ GeV and charge $(-\frac{1}{3})e$.

hadrons carrying this new flavor by photon beams. In what follows we shall assume that this quark has charge $(-\frac{1}{3}e)$, but our curves can be adjusted trivially to take into account other possibilities. We take $m_b = 5$ GeV and $m_{\text{"}D\text{"}} = 5$ GeV.

Figure 6 shows our prediction for the energy dependence of the cross section for the photoproduction of this new flavor. The curve given is for the bag-bremsstrahlung gluon distribution (2.11). We may again compare this calculation with a simple prediction based on the vector-meson-dominance model:

$$\lim_{s\to\infty}\frac{\sigma(\gamma N\to b\bar{b})}{\sigma(\gamma N\to c\bar{c})}\cong\left(\frac{\Gamma(\Upsilon(9.5)\to e\bar{e})}{m_\Upsilon}\right)\times\left(\frac{m_\psi}{\Gamma(\psi\to e\bar{e})}\right)\frac{\sigma_{\text{tot}}(\Upsilon(9.5)N)}{\sigma_{\text{tot}}(\psi N)}. \tag{2.16}$$

If we assume that $\Gamma(\Upsilon(9.5)\to e\bar{e})/\Gamma(\psi\to e\bar{e})\simeq\frac{1}{4}$ and $\sigma_{\text{tot}}(\gamma N)/\sigma_{\text{tot}}(\psi N)\sim m_\psi{}^2/m_\Upsilon{}^2$ this gives

$$\lim_{s\to\infty}\frac{\sigma(\gamma N\to b\bar{b})}{\sigma(\gamma N\to c\bar{c})}\simeq\left(\frac{1}{4}\right)\left(\frac{m_\psi}{m_\Upsilon}\right)^3\cong 10^{-2}. \tag{2.17}$$

In our QCD calculation using Eq. (2.2), we observe that the internal cross section for $\gamma(Q^2)V \to c\bar{c}$ peaks near threshold. This means that we can approximately evaluate charm production in the high-energy limit where the detailed shape of the gluon distribution is not important to obtain

$$\lim_{s\to\infty}\frac{\sigma(\gamma N\to b\bar{b})}{\sigma(\gamma N\to c\bar{c})}\simeq\left(\frac{1}{4}\right)\left(\frac{m_c}{m_b}\right)^2\frac{\alpha_s(4m_b{}^2)\ln(s/4m_b{}^2)}{\alpha_s(4m_c{}^2)\ln(s/4m_c{}^2)}, \tag{2.18}$$

where m_c and m_b are the masses of the quarks. This gives

$$\lim_{s\to\infty}\frac{\sigma(\gamma N\to b\bar{b})}{\sigma(\gamma N\to c\bar{c})}\simeq\left(\frac{1}{4}\right)\left(\frac{m_c}{m_b}\right)^2\frac{\ln(4m_c{}^2/\Lambda^2)\ln(s/4m_b{}^2)}{\ln(4m_b{}^2/\Lambda^2)\ln(s/4m_c{}^2)}$$
$$\simeq 2\times 10^{-2}\frac{\ln(s/4m_b{}^2)}{\ln(s/4m_c{}^2)} \tag{2.19}$$

for $m_c = 1.65$, $m_b = 5.0$, and $\Lambda = 0.5$ GeV. This is somewhat similar to (2.17), but it is important to note that specific GVMD models make much larger predictions for $\sigma(\gamma N \to b\bar{b})$. An estimate due to Margolis[21] is

$$\sigma(\gamma N\to b\bar{b})\sim 0.1\text{–}1\ \mu\text{b}. \tag{2.20}$$

Virtual photoproduction and deep-inelastic scattering

We now turn to the cross section for the production of charm by virtual photons. For simplicity, we calculate only the production of charm by transversely polarized photons. The transverse cross section is related to the deep-inelastic scattering structure functions by

$$\sigma_T(Q^2,\nu)=\frac{4\pi^2\alpha}{(\nu-Q^2/2m_N)}W_1^{em}(\nu,Q^2). \tag{2.21}$$

In the deep-inelastic region it is possible to interpret our results in terms of the absorption of a photon by a charmed quark or antiquark in the sea of the nucleon. We believe that for some range of length scales the sum of the first few terms in the series represented by the diagram in Fig. 7 may give a reasonable estimate for the mo-

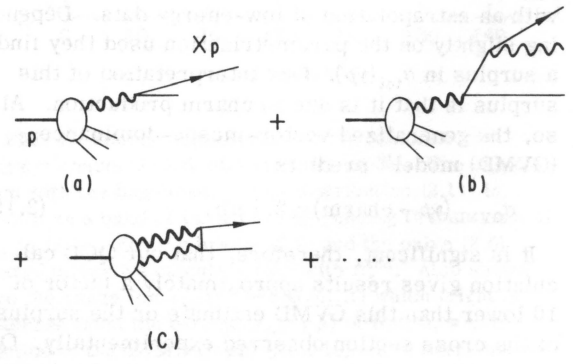

FIG. 7. Diagrams for $c\bar{c}$ pairs in the proton.

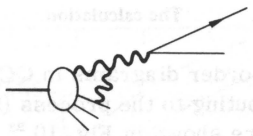

FIG. 8. Diagram for $c\bar{c}$ pair production absorbable into given momentum distribution.

mentum distribution of heavy quarks in the sea. Note that, for example, diagrams of the form of Fig. 8 are already taken into account through the choice of the gluon distribution in (2.2). Our results for $\sigma[\gamma_T(Q^2)N \to cc]$ are plotted at fixed $x_{bj} \equiv Q^2/2M_N\nu = 0.1$ as a function of Q^2 in Fig. 9. The cross section shows some evidence for scaling [$W_1(Q^2, \nu)$ a function of x_{bj} only] when $Q^2 \geq 20$ GeV^2. As in the case of real photoproduction we can compare our prediction with ones based on GVMD. According to the generalized vector-meson-dominance model, the cross section for the production of a heavy flavor is[10]

$$\sigma^{\mathrm{GVMD}}(\gamma^* N \to c\bar{c}X) = \left(\frac{3}{\alpha}\right)\Gamma(\xi \to e\bar{e})m_\xi{}^3 \frac{\sigma_{\mathrm{tot}}(\xi N)}{(\Delta m_\xi{}^2)^2} \times \zeta\left(2, \frac{m^2+Q^2}{\Delta m_\xi{}^2}\right), \quad (2.22)$$

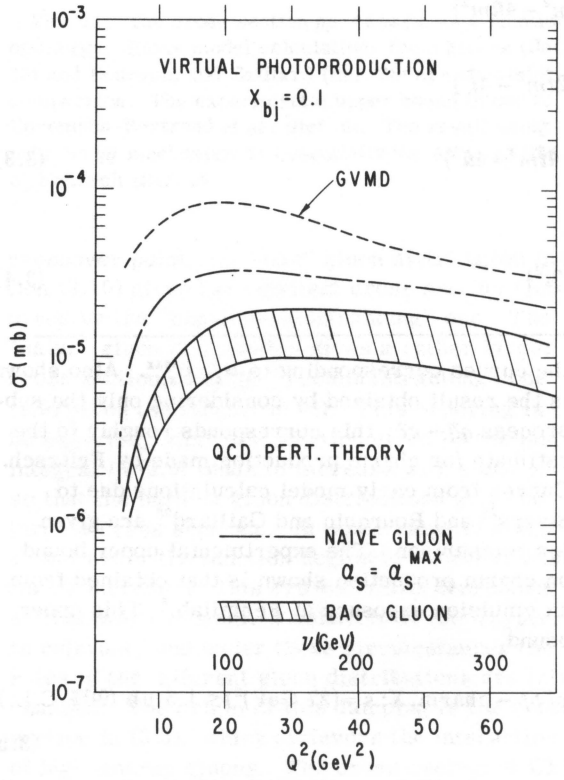

FIG. 9. The cross section for $\sigma_T\gamma(Q^2)N \to c\bar{c}, X$ for transversely polarized virtual photons at fixed $x_{bj} = Q^2/2m\nu = 0.1$. The value for QCD perturbation theory is shown with two different gluon distributions. The GVMD curve is obtained from Ref. 10.

where ξ is the lowest vector meson containing a quark and antiquark carrying the new flavor, $\Delta m_\xi{}^2$ is the splitting between vector-meson radial recurrences, and $\zeta(a, b)$ is the generalized Riemann ζ function. The series for the ζ function is truncated when $m \geq \nu$; vector mesons with larger masses should not be excited.

The magnitude of the charm-production cross section predicted by the GVMD-model calculation (2.22) is significantly larger than that implied by the present QCD calculation (2.2). This difference between the predictions of QCD and GVMD is relevant to the question of the contribution of charmed hadron production to the observed rise of the deep-inelastic structure functions with Q^2 at small x. If the GVMD estimate for charm production is correct, then a significant fraction of the apparent scaling violations observed at small x can be attributed to this process. However, our QCD calculation gives a rate which is a factor of 5–10 smaller, suggesting that it may be reasonable to interpret the experimental results for the rise in $W_2(x, Q^2)$ at small x in terms of nonscaling effects not associated with hadronic thresholds. The size of the nonscaling effects is then in rough agreement with predictions[22] based on the short-distance behavior of QCD.

Preliminary results from an experiment at Fermilab on events of the form $\mu N \to \mu\mu X$ appear to indicate that the charm production cross section is smaller than that predicted by the GVMD model and smaller than would be needed to explain the observed rise in the structure function.[1] However, a quantitative comparison of experimental results with our predictions for the charm-photoproduction cross section based on QCD is not yet possible.

III. PRODUCTION OF HEAVY HADRONS IN HADRON-HADRON COLLISIONS

In this section we consider the problem of calculating the cross section for the production of

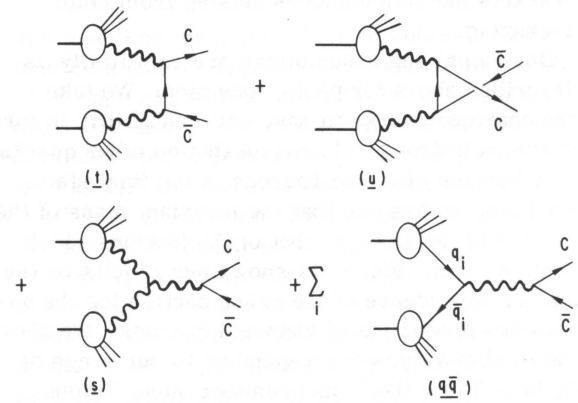

FIG. 10. Lowest-order diagrams for hadronic charm production.

massive hadrons carrying new flavors in hadron-hadron collisions. Unlike photoproduction for which there exist some sketchy experimental data with which to compare our theoretical predictions, there are, as yet, no indications of the hadronic production of charm in accelerator experiments using hadron beams.

The calculation

The lowest-order diagrams in QCD perturbation theory contributing to the process (hadron)(hadron) → charm, X are shown in Fig. 10.[23] We may write the cross section for the production of heavy quarks in the form

$$\sigma(aN \to \text{charm}, X) = \sum_{i,j} \int_{4m_D^2/s}^{1} dx\, G_{i/a}(x) \int_{4m_D^2/sx}^{1} dy\, G_{j/N}(y) \int_{\hat{t}_{\min}}^{\hat{t}_{\max}} \frac{d\hat{t}}{16\pi\hat{s}^2} |M_{ij}(\hat{s},\hat{t},\hat{u})|^2 , \tag{3.1}$$

where

$$(i,j) = (V,V),\ (q_\alpha, \bar{q}_\alpha) \text{ and } (\bar{q}_\alpha, q),\ \alpha = u,d,s, \qquad \hat{s} = xys, \tag{3.2}$$

$$\hat{t}_{\min}^{\max} = \left(\frac{2m_D^2 - \hat{s}}{2}\right) \pm \tfrac{1}{2}[\hat{s}(\hat{s} - 4m_D^2)]^{1/2} .$$

We use the quark and antiquark distributions inferred from deep-inelastic scattering data by Field and Feynman.[17] The gluon distributions we use are discussed in Sec. II. The matrix element and its calculation are presented in Appendix B. We find

$$\begin{aligned}|M(VV \to c\bar{c})(\hat{s},\hat{t},\hat{u})|^2 = {} & \frac{g^4}{(\hat{t}-m^2)^2}\left\langle\tfrac{1}{12}\right\rangle(-2m^4 - 6\hat{t}m^2 - 2\hat{u}m^2 + 2\hat{u}\hat{t}) + \frac{g^4}{(\hat{u}-m^2)^2}\left\langle\tfrac{1}{12}\right\rangle(-2m^4 - 2\hat{t}m^2 - 6\hat{u}m^2 + 2\hat{u}\hat{t}) \\ & + \frac{g^2}{\hat{s}^2}\left\langle\tfrac{3}{16}\right\rangle(-28m^4 + 20\hat{u}m^2 + 20\hat{t}m^2 - 4(\hat{t}+\hat{u})^2 + 4\hat{u}\hat{t}) \\ & + \frac{g^4}{(\hat{t}-m^2)(\hat{u}-m^2)}\left\langle-\tfrac{1}{96}\right\rangle(-8m^4 - 4\hat{t}m^2 - 4\hat{u}m^2) \\ & + \frac{g^4}{(\hat{t}-m^2)\hat{s}}\left\langle-\tfrac{3}{32}\right\rangle(-12m^4 + 4\hat{u}m^2 + 12\hat{t}m^2 - 4\hat{t}^2) \\ & + \frac{g^4}{(\hat{u}-m^2)\hat{s}}\left\langle-\tfrac{3}{32}\right\rangle(+12m^4 - 12\hat{u}m^2 - 4\hat{t}m^2 + 4\hat{u}^2)\end{aligned} \tag{3.3}$$

and

$$|M(q\bar{q} \to c\bar{c})(\hat{s},\hat{t},\hat{u})|^2 = \frac{g^4}{\hat{s}^2}\left\langle\tfrac{2}{9}\right\rangle(12m^4 - 8m^2\hat{u} - 8m^2\hat{t} + 2\hat{u}^2 + 2\hat{t}^2) , \tag{3.4}$$

where $\hat{s}, \hat{t}$, and $\hat{u}$ are the kinematic invariants for the $2 \to 2$ subprocess, m is the effective mass of the heavy quark, and $\hat{s} + \hat{t} + \hat{u} = 2m^2$. The angular brackets indicate numbers arising from color averaging.

Our remaining assumptions are essentially as described above for photoproduction. We take the charmed quarks to have unit probability to form charmed hadrons and assume that no other quarks may become charmed hadrons in the final state. Further, we assume that the invariant mass of the $c\bar{c}$ pair is the same as that of the hadrons which contain them. Figure 11 shows our results on the energy dependence of the cross section for the associated production of charmed hadrons. We show the band of values corresponding to our range of α_s in (2.7) for the "bag-bremsstrahlung" gluon distribution (2.11) while for the "naive" (2.7) and "bremsstrahlung" (2.19) distributions we given only the curves corresponding to $\alpha_s = \alpha_s^{\max}$. Also shown is the result obtained by considering only the subprocess $q\bar{q} \to c\bar{c}$; this corresponds roughly to the estimate for charm production made by Fritzsch.[24] Curves from early model calculations due to Sivers[25] and Bourquin and Gaillard[26] are given for comparison. The experimental upper bound on charm production shown is that obtained from an emulsion exposure at Fermilab.[6] This upper bound,

$$\sigma(pp \to \text{charm}, X; s = (27\ \text{GeV})^2) \lesssim 1.5\ \mu\text{b}\ (90\%\ \text{C.L.}) , \tag{3.5}$$

appears to favor small values of the strong coupling constant and/or soft gluon distributions in our model. It is significant that for $\sqrt{s} \gtrsim 40$ GeV the value obtained in the calculation is not sensitive to the shape of the gluon distribution. Below the

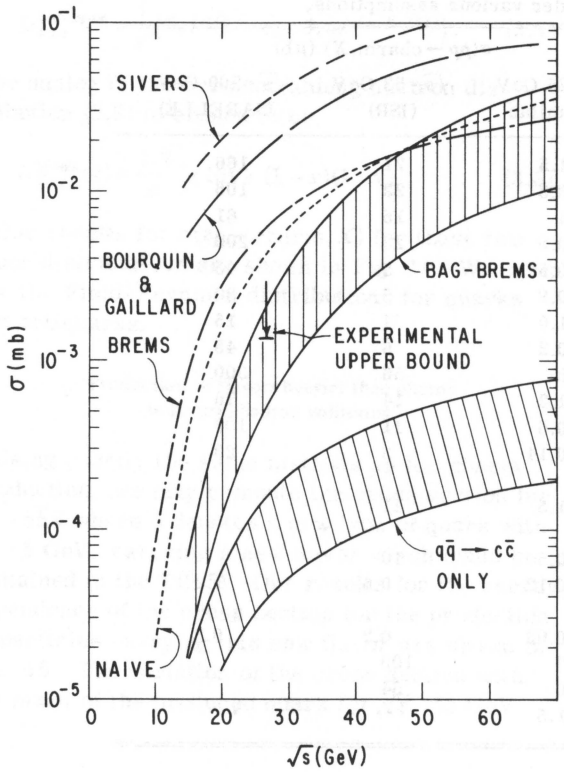

FIG. 11. The cross section $pp \rightarrow$ charm as a function of energy. Early model calculations from Sivers (Ref. 25) and Bourquin and Gaillard (Ref. 26) are shown for comparison. The experimental upper bound is due to Coremans-Bertrand *et al.* (Ref. 6). The result using only the $q\bar{q}$ mechanism is essentially the same as that of Fritzsch (Ref. 24).

crossover point, the "bag" gluon distribution function (2.10) gives the smallest cross section, followed by the "bag-bremmsstrahlung" one. The "naive" gluon distribution gives a rather larger cross section, and the "bremmsstrahlung" one (2.9) gives the largest of all. This ordering is to be expected, since the function given by the last integral in (3.6) tends to increase with x and y, so that the hardest gluon distributions give the largest cross sections. At some value of x and y, however, the function begins to decrease again. As $\sqrt{s}$ increases, this critical value decreases, so that only the small-x behavior of the $G_{V/N}(x)$ is relevant, and under these circumstances the roles of the different gluon distributions are interchanged. The origin of this damping is the cross section in (3.3), which disfavors the interaction of high-energy gluons. The cross section at CERN ISR energies is seen to be a factor of 10–20 larger than would be obtained with the $q\bar{q}$ mechanism alone. Experimental measurements in this energy range will thus be important in determining whether gluons play a role similar to partons in hadron dynamics. Table I gives our predictions for $\sigma(pp \rightarrow \text{charm}, X)$ for a variety of inputs at values of $\sqrt{s}$ corresponding to those available at various experimental facilities.

Our results also depend on the value for the charmed-quark effective mass used and, since this cannot be extracted directly from experiment, it is important to see how our prediction for the cross section depends on its value. This is shown in Fig. 12 for $\sqrt{s} = 25$. Because we are calculating the cross section for the production of quarks by hard scattering, our assumption that the effective mass of the charmed-quark pair is the same as the hadrons which contain them may be questioned. One way to test this assumption is to change the value of the threshold $s_{\text{th}} = 4m_D^2$ used in the calculation. Even if our assumption were strictly correct, we would still have to consider varying the threshold since we do not know the proportion of D's ($m_D = 1.87$ GeV), D^*'s ($m_{D^*} = 2.0$ GeV), F's ($m_F \simeq 2.1$ GeV), and F^*'s which is produced. Probably predominantly D's should be produced, because of their slightly smaller mass. The variation of the cross section with m_D effective at $\sqrt{s} = 25$ GeV is shown in Fig. 12. In view of the fact we can change our prediction by a factor of 2–3 by reasonable variations of these parameters the question of whether current experimental limits rule out a hard gluon distribution remains open. This range gives some idea of the overall sensitivity of our calculation, and therefore, if the experimental bound on the charm-hadroproduction cross section were improved by a factor of 5–10, we would find it very hard to understand in our model.

We now turn to predictions for charm production in $\bar{p}p$ and πp interactions. The quark and gluon distributions in antiprotons are easily obtained from those in protons by charge conjugation,

$$G_{V/\bar{p}}(x) = G_{V/p}(x), \qquad G_{\bar{q}_\alpha/\bar{p}}(x) = G_{q_\alpha/p}(x), \tag{3.6}$$

and inserting these into (3.1) we obtain the cross section shown in Fig. 13. The greater importance of the $q\bar{q} \rightarrow c\bar{c}$ mechanism in $\bar{p}p$ collisions is evident, but above $\sqrt{s} = 40$ GeV, $VV \rightarrow c\bar{c}$ is still the dominant mechanism in the cross section because it is almost the same as for $pp \rightarrow$ charm, X.

In order to calculate the charm-production cross section in πp collisions we must make some further assumptions regarding the π gluon distributions. In the absence of any theoretical or experimental guidance we will assume that the fraction of momentum carried by gluons is the same in the pion as it is in the nucleon. If we neglect any difference in size between the π and the N, we can obtain a gluon distribution analogous to (2.11),

TABLE I. Cross sections under various assumptions.

Input				$\sigma(pp \to \text{charm}, X)$ (μb)		
α_s	m_c (GeV)		$G_{V/p}(x)$	$\sqrt{s}=25$ GeV (Fermilab)	$\sqrt{s}=53$ GeV (ISR)	$\sqrt{s}=200$ GeV (ISABELLE)
max	1.65	2.0	Bag-brems	1.5	21	166
			Naive	3.5	22	106
			Brems	4	15	61
			Bag	0.9	23	200
min			Bag-brems	0.5	5	45
			Naive	0.9	5	30
			Brems	1.0	4	15
			Bag	0.2	6	45
max	1.4	1.75	Bag-brems	5	56	300
min				1.2	14	76
max	1.1	2.25		0.6	11	106
min				0.14	3	23
max	1.65	2.0	Bag-brems +scaling violations	1.5	41	
min				0.5	10	
max			$q\bar{q}$ only	0.12	0.6	1.2
min				0.03	0.2	0.3
Sivers model (Ref. 25)				37	100	
Borquin & Gaillard model (Ref. 26)				20	54	
Experimental bound (Ref. 6)				< 1.5	...	...

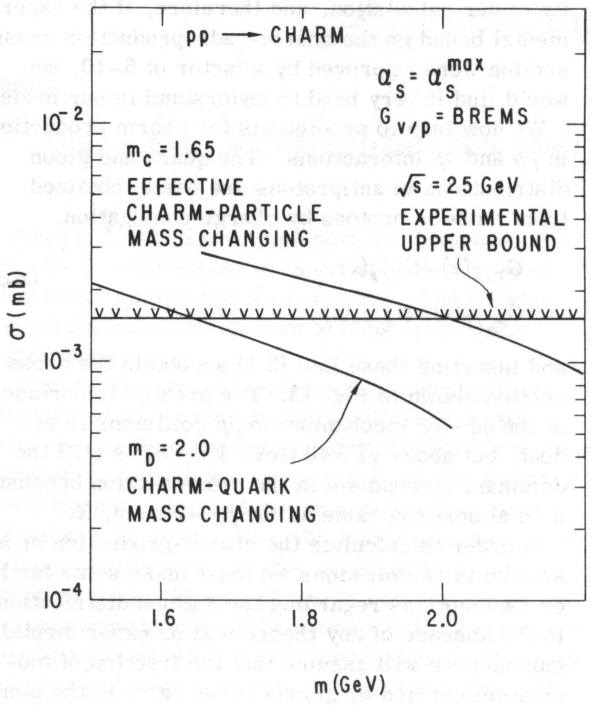

FIG. 12. Dependence of the cross section on m_c effective and m_D effective at $\sqrt{s}=25$ GeV.

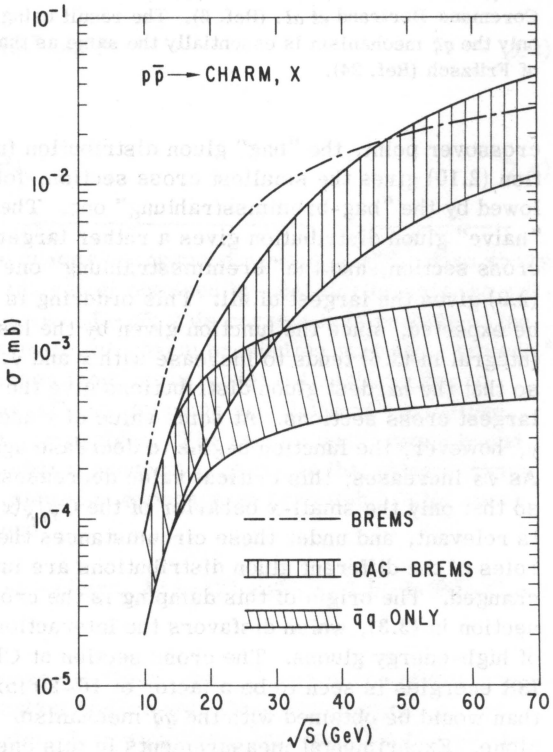

FIG. 13. Energy dependence of $\sigma(\bar{p}p \to \text{charm}, X)$ with distributions given by (3.6).

$$G_{V/\pi}^{\text{bag-brem}} = \frac{1}{x}[0.16(1-x) + 3.2e^{-(x/0.15)^2}]. \quad (3.7)$$

The analog of the bremsstrahlung nucleon distribution (2.9) is chosen to be

$$G_{V/\pi}^{\text{brems}}(x) = \frac{1.2}{x}[x \ln x + (1-x)(1+x)]. \quad (3.8)$$

Our results for $\sigma(\pi p \to \text{charm}, X)$ for these two gluon distributions are shown in Fig. 14. We again use the Field-Feynman distributions for quarks and antiquarks.

Production of flavors heavier than charm in hadron-hadron collisions

Using exactly the same methods as for charm production, we may compute the cross section for $pp \to b\bar{b}X$ where b denotes a new type of quark with $m_b = 5$ GeV, carrying a new flavor which could be contained in the $\Upsilon(9.5)$. Our results for the energy dependence of the cross section for the production of particles carrying this new flavor are shown in Fig. 15. The variation of the cross section with the mass of the produced quark for $\sqrt{s} = 53$ GeV and $\sqrt{s} = 200$ GeV is displayed in Fig. 16. For this graph we have taken $\alpha_s = \alpha_s^{\max}$ and used the "bag-bremsstrahlung" gluon distribution. From Figs. 15 and 16 one can see that the production cross section for flavors heavier than charm in hadron-hadron collisions should be quite small. Cross sections of this magnitude will be rather difficult to measure unless distinctive triggers can be found.

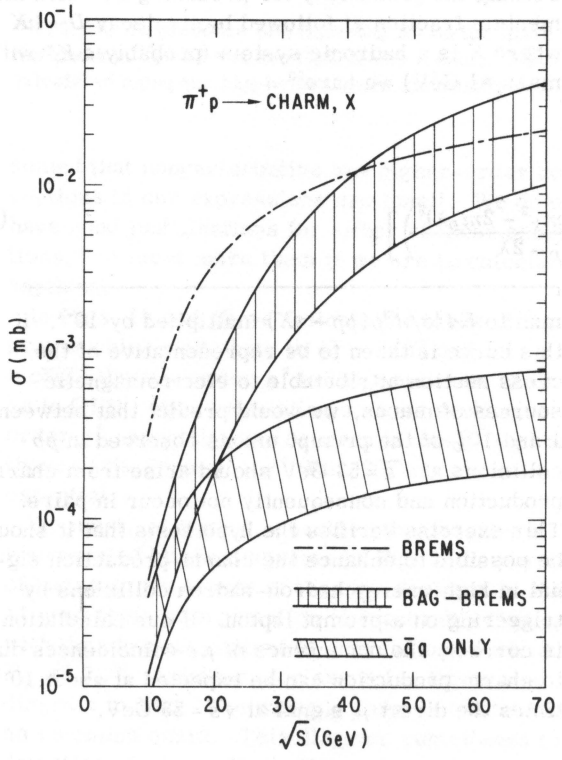

FIG. 14. Energy dependence of $\sigma(\pi p \to \text{charm}, X)$. Quark distributions are those of Field and Feynman (Ref. 17). Gluon distributions for the π are defined in (3.7) and (3.8) and for the proton in (2.11) and (2.9). If we use the "soft" bag-brems distribution for the π we also use it for the p.

Large-p_T production of charm and direct leptons

We can use the basic mechanisms illustrated in Fig. 10 to estimate the production of charmed particles at large transverse momentum (p_T). If our basic model is correct, this calculation should be somewhat more reliable than the estimate of the total charm-production cross section. The reason for this is that any final-state interactions occuring near the subprocess threshold which could be important in the evaluation of the total production cross section should not significantly affect the form of the p_T spectrum for large p_T.

We write the differential cross section for the production of a decay product (a charmed meson or a muon arising from semileptonic charmed-particle decay) of one of the charmed quarks in the form

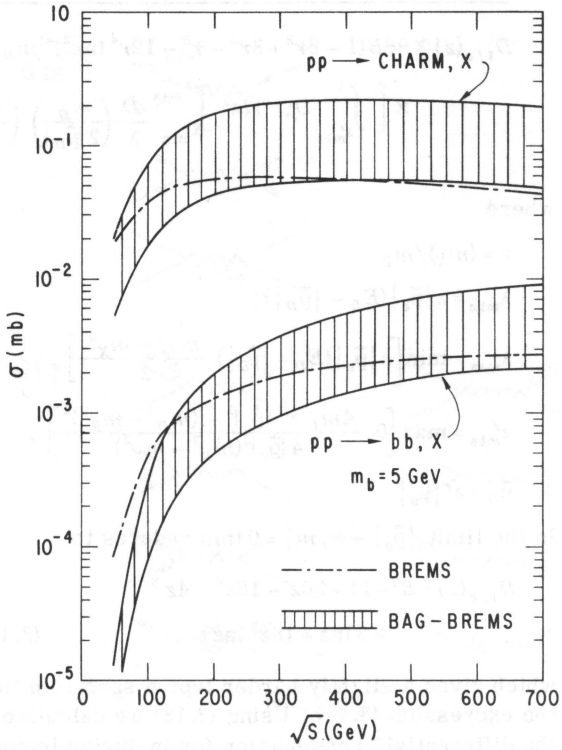

FIG. 15. Energy dependence of $\sigma(pp \to \text{charm}, X)$ and $\sigma(pp \to b\bar{b}, X)$ with $m_b = 5$ GeV in our model.

$$\frac{Ed^3\sigma(pp\to\xi x)}{d^3p}\simeq\frac{1}{\pi}\sum_{i,j}\int_{x_m}^{1}dx\,G_{i/p}(x)\int_{y_m}^{1}dy\,G_{j/p}(y)\int\frac{dz}{z^2}D_{i/c}(z)\frac{d\sigma}{d\hat{t}}(ij\to c\bar{c};\hat{s},\hat{t},\hat{u})\delta(\hat{s}+\hat{t}+\hat{u}-2m_c^2)\,, \quad (3.9)$$

where

$$\hat{s}=xys,\quad \hat{t}=xt/z,\quad \hat{u}=yu/z \quad (3.10)$$

are the Mandelstam variables for the hard-scattering subprocesses

$$x_m=\frac{2m_c^2-u}{s+t},\quad y_m=\frac{2m_c^2-xt}{xs+u} \quad (3.11)$$

and

$$z=\frac{xt+yu}{2m_c^2-xys}\,.$$

The form of (3.9) is a simple modification of the usual hard-scattering-model formula which takes into account the masses of the produced quarks. The function $D_{\xi/c}(z)$ gives the probability that the detected particle ξ carries a fraction z of the momentum of its parent charmed quark. We assume that one and only one charmed hadron arises from each charmed quark so that

$$\sum_{\xi=D,F,\ldots}\int_0^1 dz\,D_{\xi/c}(z)=1\,. \quad (3.12)$$

Since we expect the production of charmed hadrons with a small fraction of the charmed quark momentum to be negligible, we should not take

$$D_{D/c}(z)\underset{z\to 0}{\sim}\frac{1}{z} \quad (3.12)$$

as is commonly done for π production. Instead we take the simple form

$$D_{D/c}(z)=(1-z)^2 \quad (3.13)$$

suggested by constituent-counting rules.

We can also use (3.9) when ξ is a lepton (e or μ) which arises from the semileptonic decay of a charmed hadron. In this case we normalize

$$\int_0^1 dz\,D_{l/c}(z)=B(\text{“}D\text{”}\to l\nu x)\,, \quad (3.14)$$

where B is the average semileptonic branching ratio of the produced hadrons. Experimental data from e^+e^- production of charm[27] gives

$$B(D\to e\nu X)\cong 0.11\pm 0.03\,. \quad (3.15)$$

Folding the probability for producing a D with momentum fraction z' followed by its decay $D\to l\nu X$ where X is a hadronic system (probably a K^* with mass $\approx$1 GeV) we have[28]

$$D_{l/c}(z)\cong 96B(1-8r^2+8r^6-r^8-12r^4\ln r^2)^{-1}m_D^{-6}$$
$$\times\left[\int_{z'_{\min}}^{1}D(z')dz'\int_{\lambda_{\min}}^{\lambda_{\max}}\frac{d\lambda}{\lambda}\left(\frac{m_D}{2|\vec{p}_D|}\right)\left(\frac{\lambda^2(m_D^2-m_X^2-2m_D\lambda)^2}{m_D-2\lambda}\right)\right], \quad (3.16)$$

where

$$r=\langle m_X\rangle/m_D\,,$$
$$\lambda_{\min}=z|\vec{p}_c|(E_D-|\vec{p}_D|)\,,$$
$$\lambda_{\max}=\min\left[z|\vec{p}_c|(E_D+|\vec{p}_D|),\frac{m_D^2-m_X^2}{2}\right],$$
$$z'_{\min}=\max\left[0,\frac{4m_D^2z^2|\vec{p}_c|^2-(m_D^2-m_X^2)^2}{4|\vec{p}_c|^2(m_D^2-m_X^2)}\right],$$
$$\vec{p}_D=z'|\vec{p}_c|\,.$$

In the limit $|\vec{p}_c|\to\infty$, $m_X=0$ this reduces to

$$D_{l/c}(z)=B(-14+36z-18z^2-4z^3$$
$$-6\ln z+18z^2\ln z)\,, \quad (3.18)$$

which gives a slightly harder lepton spectrum than the expression (3.16). Using (3.18) we calculate the differential cross section for inclusive lepton production. This is displayed in Fig. 17. Also shown for comparison is the fit of Field and Feynman to $Ed^3\sigma/d^3p(pp\to\pi X)$ multiplied by 10^{-4}. If this curve is taken to be representative of the cross section attributable to electromagnetic sources of muons, we would predict that between 1 and 10% of the prompt muons observed in pp collisions at $\sqrt{s}=53$ GeV should arise from charm production and consequently not occur in pairs. This exercise verifies the hypothesis that it should be possible to enhance the charm-production signal in high-energy hadron-hadron collisions by triggering on a prompt lepton. If our calculation is correct, the occurrence of μe coincidences due to charm production can be expected at about 10^{-3} times the direct μ signal at $\sqrt{s}=53$ GeV.

IV. HIGHER-ORDER CORRECTIONS

In the calculation presented above, we have used lowest-order perturbation theory for our calculation of the cross section for the hard-scattering subprocesses. We have therefore implicitly as-

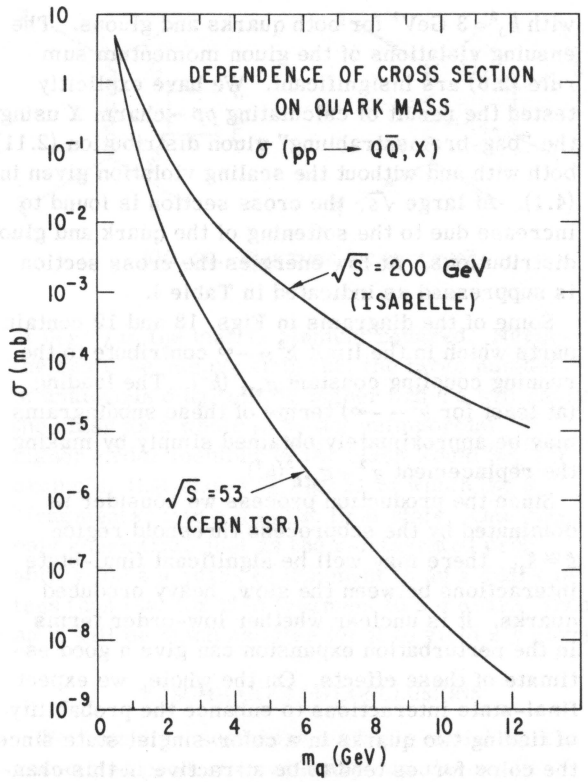

FIG. 16. Dependence of $\sigma(pp \to Q\bar{Q}, X)$ on the mass of the quark at $\sqrt{s} = 53$ and 200 GeV in our model. Curves calculated using the bag-brems gluon distribution (2.11).

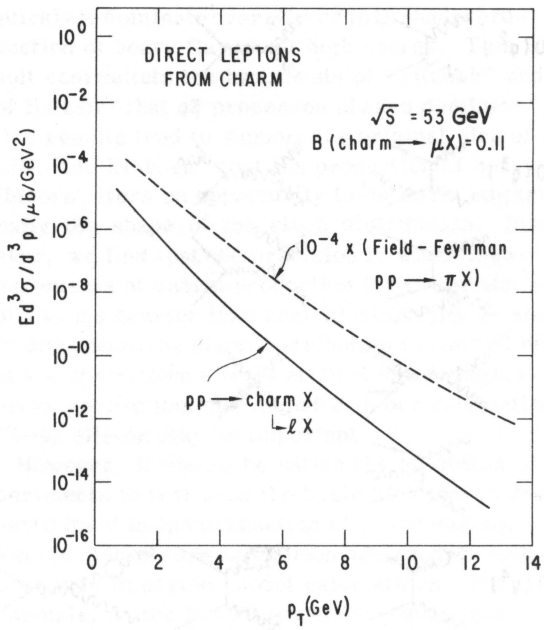

FIG. 17. Direct leptons from charmed-particle decay compared to $10^{-4} \times$(Field-Feynman $pp \to \pi x$).

sumed that nonperturbative and higher-order corrections to our expressions are small. We do not have good justifications for either of these assumptions, but must make them if we are to calculate anything.

In Figs. 18 and 19 we indicate the types of diagrams which contribute to $q\bar{q} \to c\bar{c}(X)$ and $VV \to c\bar{c}(X)$ through order g^4 in the amplitude. Just as in QED, when calculating a cross section to order g^6, cancellations between terms $g^3 \times g^3$ and those of the form $g^2 \times g^4$ (Ref. 29) are known to be essential.

We must, of course, consider the processes represented by the diagrams in Fig. 18 as portions of hadronic processes of the type depicted in Fig. 11, and their interpretation is inexorably tied up with the physical content of expressions such as Eq. (3.2).[30] Consider, for example, the second diagram in Fig. 18 in which a gluon is emitted by an incoming quark. This diagram contributes to deviations from scaling. From the analysis of scaling violations in the framework of the quark-parton model by Altarelli and Parisi[31] we may infer that the contribution of some of this diagram may be absorbed by the choice of $G_{q/n}(x)$ at the expense of allowing this to become a func-

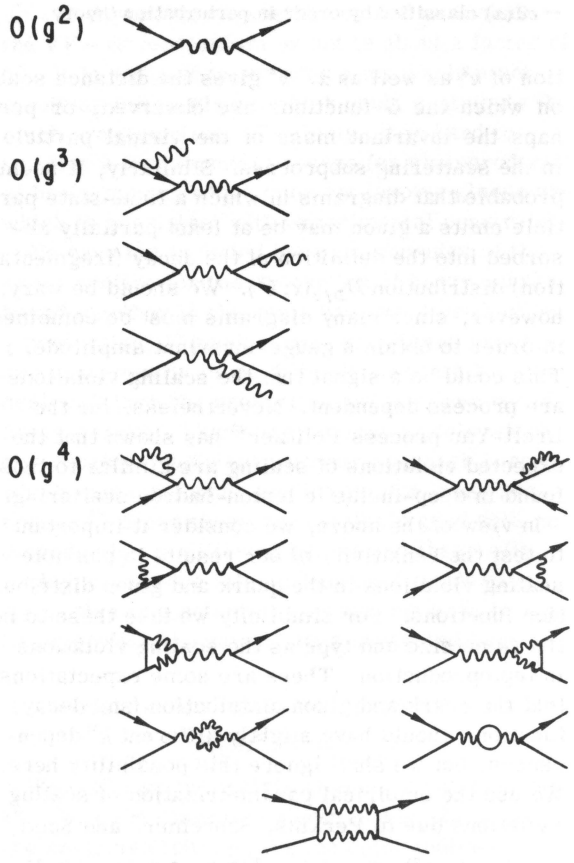

FIG. 18. Typical diagrams for the amplitude $q\bar{q} \to cc(x)$ classified by order in perturbation theory.

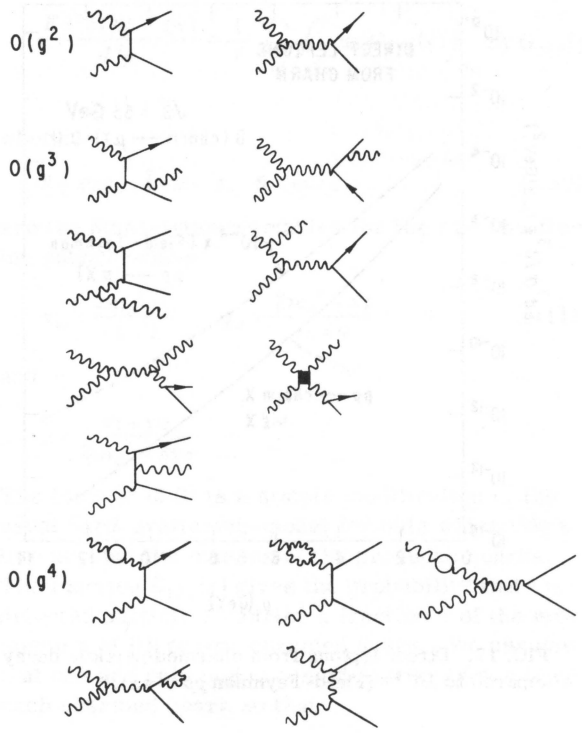

FIG. 19. Typical diagrams for the amplitude $VV \to c\bar{c}(x)$ classified by order in perturbation theory.

tion of k^2 as well as x. k^2 gives the distance scale on which the G functions are observed, or perhaps the invariant mass of the virtual particle in the scattering subprocess. Similarly, it seems probable that diagrams in which a final-state particle emits a gluon may be at least partially absorbed into the definition of the decay (fragmentation) distribution $D_{D/c}(x, k^2)$. We should be wary, however, since many diagrams must be combined in order to obtain a gauge-invariant amplitude. This could be a signal that the scaling violations are process dependent. Nevertheless, for the Drell-Yan process Politzer[32] has shown that the expected violations of scaling are similar to those found in deep-inelastic lepton-hadron scattering.

In view of the above, we consider it important to test the sensitivity of our results to possible scaling violations in the quark and gluon distribution functions. For simplicity we take these to be the same size and type as the scaling violations in leptoproduction. There are some expectations[33] that the quark and gluon distribution (and decay) functions should have slightly different k^2 dependences, but we shall ignore this possibility here. We use the empirical parametrization of scaling violations due to Perkins, Schreiner, and Scott,[34]

$$G_{i/N}(x, k^2) = G_{i/N}(x) \exp[(0.2 - 0.9x) \ln k^2/k_0^2], \tag{4.1}$$

with $k_0^2 = 3$ GeV^2 for both quarks and gluons. The ensuing violations of the gluon momentum sum rule (2.6) are insignificant. We have explicitly tested the result of calculating $pp \to$ charm X using the "bag-bremsstrahlung" gluon distribution (2.11) both with and without the scaling violation given in (4.1). At large $\sqrt{s}$, the cross section is found to increase due to the softening of the quark and gluon distributions. At low energies the cross section is suppressed as indicated in Table I.

Some of the diagrams in Figs. 18 and 19 contain parts which in the limit $k^2 \to -\infty$ contribute to the running coupling constant $g_{\text{eff}}^2(k^2)$. The leading (at least for $k^2 \to -\infty$) terms of these subdiagrams may be approximately obtained simply by making the replacement $g^2 \to g_{\text{eff}}^2(k^2)$.

Since the production process we consider is dominated by the subprocess threshold region $\hat{s} \cong \hat{s}_{\text{th}}$, there may well be significant final-state interactions between the slow, heavy produced quarks. It is unclear whether low-order terms in the perturbation expansion can give a good estimate of these effects. On the whole, we expect final-state interactions to enhance the probability of finding two quarks in a color-singlet state since the color forces tend to be attractive in this channel. Evidence for this is seen in the production of charm in e^+e^- annihilation where resonances and other effects raise the cross section above the value predicted by the naive parton model. In contrast, repulsive final-state interactions between $c\bar{c}$ in a color-octet state should depress the cross section. Since our model for $\gamma_T(Q^2)N \to c\bar{c}$ produces only color octets we may be overestimating the cross section by neglecting final-state interactions near threshold. In hadronic production the mechanism $VV \to c\bar{c}$ produces a mixture of singlets and octets and there should be both attractive and repulsive corrections. We have tested for the effect of final-state interactions by changing the effective quark mass (and hence moving the subprocess threshold) as discussed in Sec. III. We have also inserted oscillations in the cross section near threshold representing resonances, but these did not change the overall result by more than a few percent indicating that it is gluon distribution functions which represent the most sensitive part of the calculation for the cross section. One particular class of diagrams deserves further attention. The first of these qualitatively new diagrams appears at $O(g^4)$ and at $O(g^6)$ a large number of this class of diagram occur. Examples are given in Fig. 20. Their distinguishing feature is that it is gluons or light quarks which undergo hard scattering but these generate a $c\bar{c}$ pair in the final state. Note that, because of their unusual final states, such diagrams will only occur

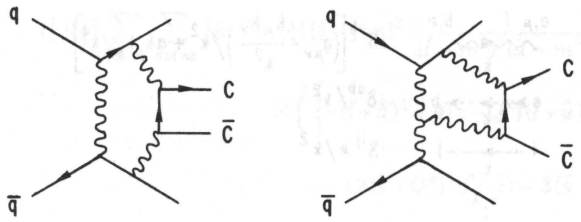

FIG. 20. Diagrams for $qq \to qqc\bar{c}$.

at $0(g^{12})$ in the matrix element squared. Nevertheless it seems possible that the large number of analogous diagrams in higher orders will cause the class as a whole to be not unimportant. A higher-order member of the class would be, for example, that shown in Fig. 21 in which the q "fragments" into a c in the final state. One may only guess that, just as the z-integrated probability for a u quark to fragment to an s quark is less than that for it to fragment to a d quark, then so it will be much smaller for it to yield a c quark.

V. SUMMARY AND CONCLUSIONS

We have discussed here a simple model for the associated production of heavy new flavors in photon-hadron and hadron-hadron collisions. Our fundamental assumption is that the subprocesses of lowest order in the QCD perturbation series dominate the production of heavy quarks. For real and virtual photoproduction this fixes the internal mechanism to be $\gamma(Q^2)V \to c\bar{c}$ while for hadron-hadron collisions we consider a mixture of $q\bar{q} \to c\bar{c}$ and $VV \to c\bar{c}$.

The major unknown quantity in the calculations is the shape of $G_{V/N}(x)$, the distribution of vector gluons in a nucleon. We calculate with a range of shapes for this function discussed earlier in the context of QCD gluon contributions to large-p_T production. With this range for the input gluon distributions, the internal process $VV \to c\bar{c}$ is found quickly to dominate over $q\bar{q} \to c\bar{c}$ in the hadroproduction of heavy flavors at high energy. This result contradicts the hypothesis of Fritzsch[24] and of Halzen[35] that $q\bar{q}$ processes always dominate. Our results tend to support the original idea of Ellis and Einhorn[36] that the production of heavy flavors offers an opportunity to estimate empirically the shape of the gluon distribution. However, we find that the precision to which measurements of charm production (or the production of flavors heavier than charm) can really be said to determine the gluon distribution is limited because of unknown effects attributable to higher-order corrections not included in our calculation. These effects may be important.

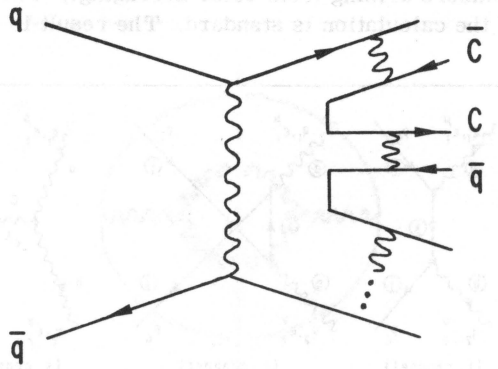

FIG. 21. Higher-order diagram for $qq \to qqc\bar{c} \cdots$.

However, it should be within the capability of experiments to test soon the basic idea that gluons participate in the production of heavy quarks. Vector gluons have often been assigned an ambiguous role in parton-model calculations. For example, in the constituent-interchange model for large-p_T production, gluon exchange is used to determine the shape of quark distributions, but gluons are not considered in that model to be constituents themselves.[37] In our approach, the difference in the cross section for $pp \to \text{charm}, X$ at $\sqrt{s} = 53$ depending on whether or not we include the $VV \to c\bar{c}$ mechanism or not is about a factor of 50. It is difficult to envision a mechanism not involving initial gluons which could contribute this much cross section. Similarly, it is hard to imagine a fundamental process for photoproduction of heavy quarks which does not involve gluons and which is consistent with experimental constraints.

We have not included here a discussion of the cross section for the production of heavy quarks bound together in the same hadron, ψ production, χ production, Υ production, etc. These processes are conceptually more difficult since we have to deal with both the production and confinement of heavy quarks. There are several models which are roughly consistent with our approach here which make different predictions for these processes.[38] Since there are available good data on ψ production in different beams and there will probably be more information on Υ production soon, this is a potentially rewarding area in which to generalize the calculations presented here.

APPENDIX A: MATRIX ELEMENT FOR THE PROCESS $\gamma_T(Q^2)V \to \bar{c}c$

We consider the matrix element represented by the Feynman diagrams shown in Fig. 22, where the encircled letters give the color indices of the particles and run from 1 to 3 for quarks and antiquarks and from 1 to 8 for gluons. Using the

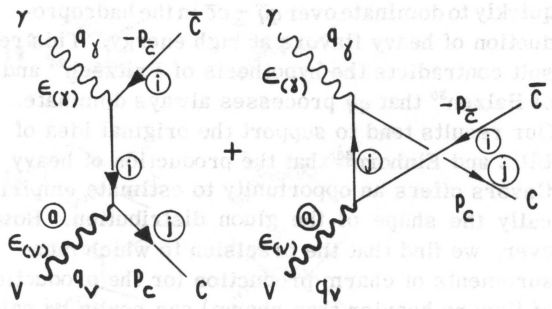

FIG. 22. Diagrams for $\gamma V \to c\bar{c}$.

Feynman rules for QCD summarized in Fig. 23 we find for the matrix element

$$M = \tfrac{2}{3} e g \bar{u}(p_c)\left\{\frac{T^b_{ij}\not{\epsilon}_{(v)}[(\not{q}_\gamma - \not{p}_{\bar{c}}) + m]\not{\epsilon}_{(\gamma)}}{(\hat{t} - m^2)} + T^b_{ij}\not{\epsilon}_{(\gamma)}\frac{[(\not{q}_v - \not{p}_{\bar{c}}) + m]\not{\epsilon}_{(v)}}{(\hat{u} - m^2)}\right\} u(p_{\bar{c}}), \quad \text{(A1)}$$

where $\epsilon_{(\gamma)}$ and $\epsilon_{(v)}$ are, respectively, the polarization vectors for the photon and gluon and

$$\hat{s} = (q_\gamma + q_v)^2 = (p_c + p_{\bar{c}})^2,$$
$$\hat{t} = (q_\gamma - p_{\bar{c}})^2 = (p_c - q_v)^2, \quad \text{(A2)}$$
$$\hat{u} = (q_v - p_{\bar{c}})^2 = (p_c - q_\gamma)^2,$$
$$\hat{s} + \hat{t} + \hat{u} = 2m^2 + q_\gamma{}^2 = 2m^2 - Q^2. \quad \text{(A3)}$$

As always, m is the effective mass of the charmed quark (c) and $-Q^2 = q_\gamma{}^2$ is the virtual-photon invariant mass squared (γ refers to both real and virtual photons). The factor $(\frac{2}{3})$ denotes the charge of the quark in units of the electron charge.

The matrix element M can be written in the following form:

$$M = \epsilon^\mu_{(v)}\epsilon^\nu_{(\gamma)} M_{\mu\nu}, \quad \text{(A4)}$$

which gives

$$\tfrac{1}{4}\left(\sum_{\lambda v}\epsilon^\mu_{(v)}\epsilon^{\alpha *}_{(v)}\right)\left(\sum_{\lambda\gamma}\epsilon^\nu_{(\gamma)}\epsilon^{\beta *}_{(\gamma)}\right) M_{\mu\nu} M^*_{\alpha\beta} \quad \text{(A5)}$$

upon squaring and averaging over photon and gluon polarizations. We calculate the cross section for (transverse) real gluons and (transverse) real and *transverse* virtual photons. The sum over gluon helicities (λv) simply gives a $-g^{\mu\alpha}$, while the sum over photon helicities ($\lambda\gamma$) gives a $-g^{\nu\beta}$ for real photons and $R^{\nu\beta}(q_\gamma q_v)$ for virtual ones where

$$R^{\nu\beta}(q_\gamma, q_v) = -g^{\nu\beta} + \frac{[(q_\gamma \cdot q_v)(q_\gamma{}^\nu q_v{}^\beta + q_\gamma{}^\beta q_\gamma{}^\nu) - q_\gamma{}^2 q_v{}^\nu q_v{}^\beta]}{(q_\gamma \cdot q_v)^2}. \quad \text{(A6)}$$

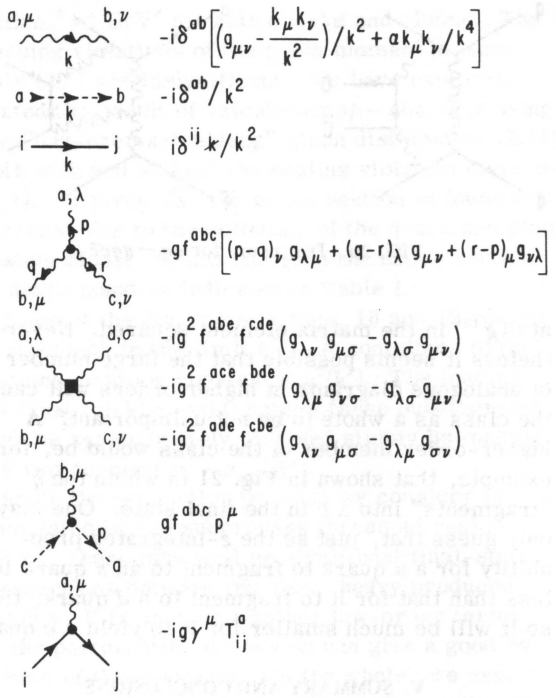

FIG. 23. The Feynman rules for QCD perturbation theory.

The $R^{\nu\beta}(q_\gamma, q_v)$ assures transversality for the proton in the virtual-photon–gluon center-of-momentum frame.

The numerical factor arising from the sum over final color and the average over initial color degrees of freedom is simple in this case since the color matrix element T^b_{ij} may be factored from both t- and u-channel matrix elements so that the complete color factor in the squares of the matrix elements becomes

$$\tfrac{1}{8}\sum_{b,\,i,\gamma} T^b_{ij}\, T^{b*}_{ij} = \langle \tfrac{1}{2} \rangle. \quad \text{(A7)}$$

(We shall throughout put angular brackets around numbers arising from color averaging.) The rest of the calculation is standard. The result is

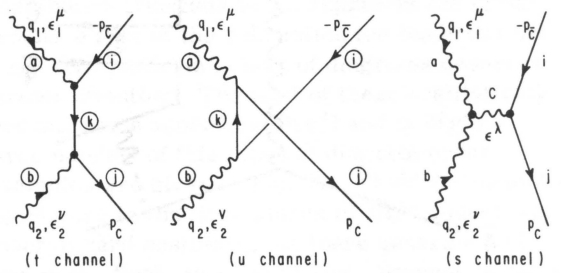

FIG. 24. Diagrams for $VV \to c\bar{c}$.

$$(\tfrac{1}{8})(\tfrac{1}{4})\sum_{\text{color}}\sum_{\text{spins}}|M|^2=\langle\tfrac{1}{2}\rangle(\tfrac{1}{4})(\tfrac{2}{3}eg)^2\frac{1}{(\hat{t}-m^2)^2(\hat{u}-m^2)^2}$$
$$\times\left(\left\{-(\hat{t}+\hat{u})^4-4(\hat{s}+Q^2)(\hat{t}+\hat{u})(\hat{t}-\hat{u})^2-4(\hat{s}+Q^2)^2[(\hat{t}-\hat{u})^2+2(\hat{t}+\hat{u})^2]\right.\right.$$
$$\left.-12(\hat{s}+Q^2)^3(\hat{t}+\hat{u})-3(\hat{s}+Q^2)^4\right\}$$
$$+\left(\frac{Q^2}{\hat{s}+Q^2}\right)[2(\hat{t}-\hat{u})^4+8(\hat{s}+Q^2)(\hat{t}+\hat{u})(\hat{t}-\hat{u})^2+8(\hat{s}+Q^2)^2(\hat{t}-\hat{u})^2-2(\hat{s}+Q^2)^4]$$
$$\left.+\left(\frac{Q^2}{\hat{s}+Q^2}\right)^2[-2(\hat{t}-\hat{u})^4+2(\hat{s}+Q^2)^4]\right)$$

This formula is appropriate for both virtual photons with $q^2=-Q^2<0$ and real photons (after setting $Q^2=0$).

APPENDIX B: MATRIX ELEMENTS FOR THE PROCESSES $VV\to c\bar{c}$ AND $q\bar{q}\to c\bar{c}$

The lowest-order Feynman diagrams for the process $VV\to c\bar{c}$ are shown in Fig. 24 and the corresponding matrix element is

$$M=g^2\bar{u}(p_c)\left\{T^a_{ik}T^b_{kj}\frac{\not\epsilon_2[(\not q_1-\not p_{\bar c})+m]\not\epsilon_1}{(\hat{t}-m^2)}+T^b_{ik}T^a_{kj}\frac{\not\epsilon_1[(\not q_2-\not p_{\bar c})+m]\not\epsilon_2}{(\hat{u}-m^2)}\right.$$
$$\left.+if^{abc}C^{\mu\nu\lambda}(-q_1,-q_2,q_1+q_2)\frac{\epsilon_{1\mu}\epsilon_{2\nu}}{\hat{s}}\gamma_\lambda T^c_{ij}\right\}v(p_{\bar c}), \tag{B1}$$

where $C^{\mu\nu\lambda}(-q_1,-q_2,q_1+q_2)$ is the three-gluon vertex defined in Fig. 23, and

$$\hat{s}=(q_1+q_2)^2=(p_c+p_{\bar c})^2,$$
$$\hat{t}=(q_1-p_{\bar c})^2=(p_c-q_2)^2, \tag{B2}$$
$$\hat{u}=(q_2-p_{\bar c})^2=(p_c-q_1)^2.$$

Once again, we can write M as $\epsilon_1^\mu\epsilon_2^\nu M_{\mu\nu}$ and

$$\frac{1}{4}\sum_{\substack{\text{gluon}\\ \text{helicities}}}|M|^2=\frac{1}{4}\left(\sum_{\lambda_1}\epsilon_1^\mu\epsilon_1^{\alpha *}\right)\left(\sum_{\lambda_2}\epsilon_2^\nu\epsilon_2^{\beta *}\right)M_{\mu\nu}M_{\alpha\beta}. \tag{B3}$$

The true sum over polarization states is given by

$$\sum_{\lambda_1}\epsilon_1^\mu\epsilon_1^{\alpha *}=R^{\mu\alpha}(q_1,q_2) \tag{B4}$$

and

$$\sum_{\lambda_2}\epsilon_2^\nu\epsilon_2^{\beta *}=R^{\nu\beta}(q_2,q_1), \tag{B5}$$

where

$$R^{\mu\alpha}(q_1q_2)=-g^{\mu\alpha}+\frac{2}{s}(q_1^\mu q_2^\alpha+q_1^\alpha q_2^\mu). \tag{B6}$$

If the two polarization sums are taken as $g^{\mu\alpha}$ and $g^{\nu\beta}$, respectively, then using the trace indicated in Fig. 25 for the $|\underline{s}|^2$ term in the matrix element squared, in which a closed loop occurs, two further diagrams containing "ghosts" must be added. These are shown in Fig. 26. Ghost terms, in fact, may be avoided by using one full

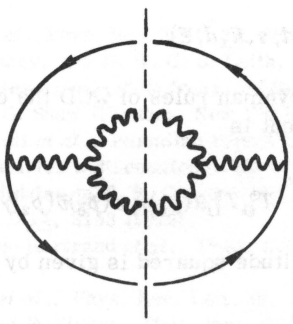

FIG. 25. Gluon loop for polarization sum.

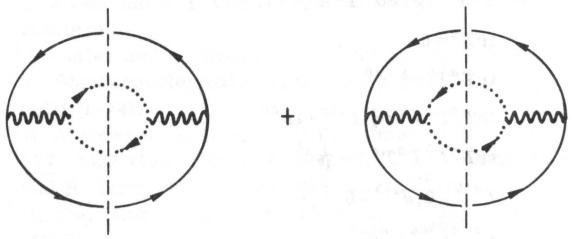

FIG. 26. Ghost loops for polarization sum.

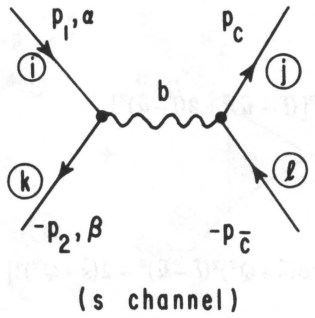

FIG. 27. Diagram for $q\bar{q} \to c\bar{c}$.

polarization since gauge invariance demands that

$$\epsilon_1^\mu q_2^\nu M_{\mu\nu} = q_1^\mu \epsilon_2^\nu M_{\mu\nu} = 0 . \tag{B7}$$

This was verified by explicit computation. The calculation was done in two ways: first with $R^{\mu\alpha}(q_1, q_2)(-g^{\nu\beta})M_{\mu\nu}M_{\alpha\beta}$ and second using $(-g^{\mu\alpha})(-g^{\nu\beta})M_{\mu\nu}M_{\alpha\beta}$ + ghost terms. The same result was obtained by both methods, but the answer presented here is in the form obtained directly from the second one.

It is convenient, because of the different color matrices in (B1), to express the matrix element squared in the form

$$|\bar{M}|^2 = |\underline{t}|^2 + |\underline{u}|^2 + |\underline{s}|^2 + 2\,\mathrm{Re}(\underline{t}^*\underline{u}) + 2\,\mathrm{Re}(\underline{u}^*\underline{s}) + 2\,\mathrm{Re}(\underline{s}^*\underline{t}) . \tag{B8}$$

For example, the color factor for the $|\underline{t}|^2$ term is

$$\left(\frac{1}{8^2}\right) \sum_{ab} \sum_{kk'} \sum_{ij} T^a_{ik} T^a_{k'i} T^b_{kj} T^b_{jk'} = \left\langle \tfrac{1}{12} \right\rangle . \tag{B9}$$

Other examples of color sums are presented in Appendix C. The explicit ghost term used was

TABLE II. Identities for matrix representations of SU(3). I represents the 3×3 identity matrix.

$T^a = \frac{\lambda^a}{2}$ where λ^a are Gell-Mann matrices
$[T^a, T^b] = if^{abc}T^c$
$\{T^a, T^b\} = \frac{1}{3}\delta^{ab}I + d^{abc}T^c$
$T^aT^b = \frac{1}{2}(\frac{1}{3}\delta^{ab}I + d^{abc} + if^{abc}T^c)$
$\mathrm{tr}T^a = 0$
$\mathrm{tr}T^aT^b = \frac{1}{2}\delta^{ab}$
$\mathrm{tr}T^aT^bT^c = \frac{1}{4}d^{abc} + if^{abc}$
$\mathrm{tr}T^aT^bT^aT^c = -\frac{1}{12}\delta^{bc}$
$f^{abb} = 0, d^{abb} = 0$
$f^{acd}f^{bcd} = 3\delta^{ab}$

$$|\mathrm{ghost}|^2 = \left\langle \frac{3}{16} \right\rangle \left(\frac{1}{4}\right) \frac{g^2}{\hat{s}^2} (-1)2 ,$$

$$\mathrm{tr}[(p_c + m)\not{q}_1(\not{p}_{\bar{c}} - m)(-\not{q}_2)] = -\left(\frac{1}{2}\right) g^4 \left\langle \frac{3}{16} \right\rangle \left[\frac{1 - (\hat{u} - m^2)^2 + (\hat{t} - m^2)^2}{\hat{s}^2}\right] .$$

Finally we have

$$|M|^2 = |\underline{t}|^2 + |\underline{u}|^2 + |\underline{s}|^2 + 2\,\mathrm{Re}(\underline{t}^*\underline{u}) + 2\,\mathrm{Re}(\underline{u}^*\underline{s}) + 2\,\mathrm{Re}(\underline{s}^*\underline{t}) ,$$

where

$$|\underline{t}|^2 = \frac{g^4}{(\hat{t} - m^2)^2} \left\langle \tfrac{1}{12} \right\rangle [-14m^4 + (8\hat{u} + 6\hat{s})m^2 - 2\hat{u}(\hat{u} + \hat{s})] ,$$

$$|\underline{u}|^2 = \frac{g^4}{(\hat{u} - m^2)^2} \left\langle \tfrac{1}{12} \right\rangle [-6m^4 + 2\hat{s}m^2 - 2\hat{u}(\hat{u} + \hat{s})] ,$$

$$|\underline{s}|^2 = \frac{g^4}{\hat{s}^2} \left\langle \tfrac{3}{16} \right\rangle \{-4m^4 + (8\hat{u} - 4\hat{s})m^2 - 4[\hat{s}^2 + \hat{u}(\hat{u} + \hat{s})]\} , \tag{B10}$$

$$2\,\mathrm{Re}(\underline{t}^*\underline{u}) = \frac{g^4}{(\hat{t} - m^2)(\hat{u} - m^2)} \left\langle -\tfrac{1}{96} \right\rangle (-16m^4 + 4\hat{s}m^2) ,$$

$$2\,\mathrm{Re}(\underline{u}^*\underline{s}) = \frac{g^4}{(\hat{u} - m^2)\hat{s}} \left\langle -\tfrac{2}{32} \right\rangle (4m^4 - 8\hat{u}m^2 + 4\hat{s}m^2 + 4\hat{u}^2) ,$$

$$2\,\mathrm{Re}(\underline{s}^*\underline{t}) = \frac{g^4}{(\hat{t} - m^2)\hat{s}} \left\langle \tfrac{3}{32} \right\rangle (-4m^4 + 8\hat{u}m^2 + 4\hat{s}m^2 - 4\hat{u}^2 - 4\hat{s}^2 - 8\hat{u}\hat{s}) .$$

Note that the particular division of terms here is that coming directly from a calculation involving ghost terms. The division depends on the gauge used, and no single term should be considered on its own. The Feynman diagram for the process $q\bar{q} \to c\bar{c}$ is shown in Fig. 27, where α and β are flavor indices

$$\alpha, \beta = (u, d, s, \bar{u}, \bar{d}, \bar{s}) .$$

Using the Feynman rules of QCD the corresponding matrix element is

$$M = \delta_{\alpha\beta} \frac{g^2}{\hat{s}} T^b_{ik} T^b_{lj} \bar{u}(p_c)\gamma_\mu v(p_{\bar{c}})\bar{v}(p_2)\gamma^\mu u(p_1) ,$$

and the amplitude squared is given by

$$|\bar{M}|^2 = \frac{g^4}{\hat{s}^2} \left\langle \tfrac{2}{9} \right\rangle [2(\hat{t}^2 + \hat{u}^2) - 8m^2(\hat{u} + \hat{t}) + 12m^4] .$$

APPENDIX C: COLOR SUMS

We give explicitly the color sums associated with the various terms in Eq. (B10) (all repeated indices are summed over).

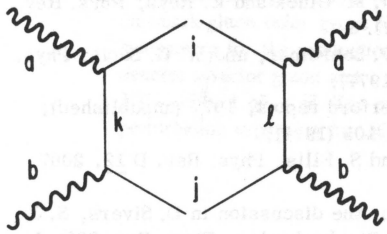

$$T^a_{ik}T^b_{kj}T^b_{jl}T^a_{li} = \mathrm{tr}(T^aT^bT^bT^a) = \tfrac{16}{3}$$

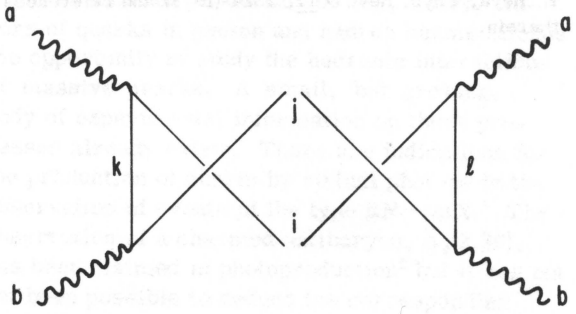

$$T^b_{ik}T^a_{kj}T^a_{jl}T^b_{li} = \mathrm{tr}(T^bT^aT^aT^b) = \tfrac{16}{3}$$

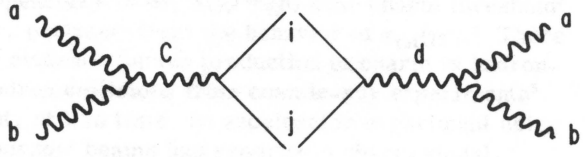

$$f^{abc}T^c_{ij}T^d_{jl}f^{abd} = f^{abc}f^{abd}\,\mathrm{tr}(T^cT^d) = 12$$

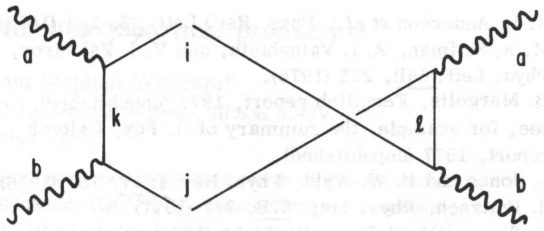

$$T^a_{ik}T^b_{kj}T^a_{jl}T^b_{li} = \mathrm{tr}(T^aT^bT^aT^b) = -\tfrac{2}{3}$$

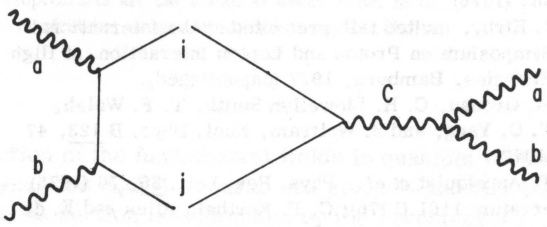

$$T^a_{ik}T^b_{kj}T^c_{ji} - if^{abc} = -if^{abc}\,\mathrm{tr}(T^aT^bT^c) = 6$$

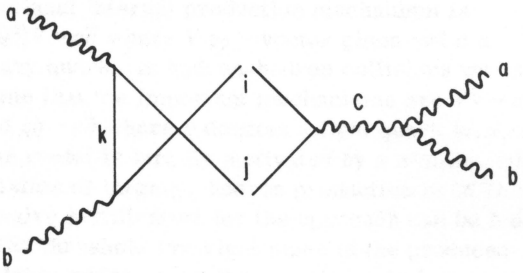

$$T^b_{ik}T^a_{kj}T^c_{ji} - if^{abc} = -if^{abc}\,\mathrm{tr}(T^bT^aT^c) = -6$$

The color factors in angular brackets in the text are obtained by dividing the above color sums by 8^2 to average over initial color states.

Table II gives the identities for matrix representations of SU(3) used to derive the color sums given above.

---

*Present address: Physics Department, California Institute of Technology, Pasadena, California 91125.

[1]W. Chen, in *Proceedings of the International Symposium on Lepton and Photon Interactions at High Energies, Hamburg, 1977,* edited by F. Gutbrod (DESY, Hamburg, 1977).

[2]B. Knapp *et al.*, Phys. Rev. Lett. 37, 882 (1976).

[3]For a summary, see D. W. G. S. Leith, in *Electromagnetic Interactions of Hadrons*, edited by A. Donnachie and G. Shaw (Plenum, New York, 1977).

[4]D. O. Caldwell *et al.*, Fermilab report (unpublished).

[5]See, for example, a discussion of the cosmic-ray charm candidates in T. K. Gaisser and F. Halzen, Phys. Rev. D 14, 3153 (1976).

[6]G. Coremans-Bertrand *et al.*, Phys. Lett. 65B, 480 (1976).

[7]S. W. Herb *et al.*, Phys. Rev. Lett. 39, 252 (1977).

[8]R. Cutler and D. Sivers, Phys. Rev. D 17, 196 (1978).

[9]B. L. Combridge, J. Kripfganz, and J. Ranft, Phys. Lett. 70B, 234 (1977).

[10]F. E. Close, D. M. Scott, and D. Sivers, Nucl. Phys. B117, 134, (1976).

[11]S. Okubo, Phys. Lett. 5, 160 (1963); G. Zweig, report, 1964 (unpublished); J. Iizuka, Prog. Theor. Phys. Suppl. 37-38, 21 (1966).

[12]D. Sivers, J. Townsend, and G. West, Phys. Rev. D 13, 1234 (1976).

[13]L. Jones and H. W. Wyld, Illinois report, 1977 (unpublished).

[14]R. Cutler and D. Sivers, Phys. Rev. D 16, 679 (1977).

[15]R. Blankenbecler and S. J. Brodsky, Phys. Rev. D 10, 2973 (1974).

[16]H. Abarbanel, S. Drell, and F. Gilman, Phys. Rev. 177, 2458 (1969); P. V. Landshoff, J. C. Polkinghome, and R. Short, Nucl. Phys. B28, 225 (1971).

[17]R. Field and R. Feynman, Phys. Rev. D 15, 2590 (1970).

[18]B. Knapp *et al.*, Phys. Rev. Lett. 34, 1040 (1975).

[19]R. L. Anderson *et al.*, Phys. Rev. Lett. 38, 263 (1977).
[20]M. A. Shifman, A. I. Vainshtein, and V. I. Zakharov, Phys. Lett. 65B, 255 (1976).
[21]B. Margolis, Fermilab report, 1977 (unpublished).
[22]See, for example, the summary of G. Fox, Caltech report, 1977 (unpublished).
[23]L. Jones and H. W. Wyld, Phys. Rev. D 17, 759 (1978).
[24]H. Fritzsch, Phys. Lett. 67B, 217 (1977).
[25]D. Sivers, Nucl. Phys. B106, 95 (1976).
[26]M. Bourquin and J. M. Gaillard, Nucl. Phys. B114, 334 (1976).
[27]J. Kirby, invited talk presented at the International Symposium on Proton and Lepton Interactions at High Energies, Hamburg, 1977 (unpublished).
[28]M. Gronau, C. H. Llewellyn Smith, T. F. Walsh, T. C. Yang, and S. Wolfram, Nucl. Phys. B 123, 47 (1977).
[29]T. Appelquist *et al.*, Phys. Rev. Lett. 36, 76 (1976) erratum 1161 (1976); C. P. Korthals Altes and E. de Rafael, Phys. Lett. 62B, 320 (1976).
[30]J. M. Cornwall and G. Tiktopoulos, Phys. Rev. Lett. 35, 338 (1975); and Phys. Rev. D 13, 3370 (1976).
[31]G. Altarelli and G. Parisi, LPTENS Report No. 77/6, 1977 (unpublished).
[32]H. D. Politzer, Harvard report, 1977 (unpublished).
[33]See, for example, A. Buras and K. Gaemers, Nucl. Phys. B132, 249 (1978); M. Glück and E. Reya, Phys. Rev. D 16, 3242 (1977).
[34]D. H. Perkins, P. Schreiner, and W. G. Scott, Phys. Lett. 67B, 347 (1977).
[35]F. Halzen, Rutherford report, 1977 (unpublished); Phys. Lett. B69, 105 (1977).
[36]M. B. Einhorn and S. Ellis, Phys. Rev. D 12, 2007 (1975).
[37]See, for example, the discussion in D. Sivers, S. J. Brodsky, and R. Blankenbecler, Phys. Rep. 23C, 1 (1976).
[38]See, for example, M. Glück, J. F. Owens, and E. Reya, Phys. Rev. D 17, 2324 (1978) and references therein.